Title

Retinal waves regulate afferent terminal targeting in the early visual pathway

Journal

Proceedings of the National Academy of Sciences of the United States of America, 112(22)

ISSN

0027-8424

Authors

Failor, Samuel
Chapman, Barbara
Cheng, Hwai-Jong

Publication Date

2015-06-02

DOI

10.1073/pnas.1506458112

Peer reviewed

Retinal waves regulate afferent terminal targeting in the early visual pathway

Samuel Failor[a,1], Barbara Chapman[a,b,2], and Hwai-Jong Cheng[a,b,c,3]

[a]Center for Neuroscience, University of California, Davis, CA 95618; [b]Department of Neurobiology, Physiology, and Behavior, University of California, Davis, CA 95616; and [c]Department of Pathology and Laboratory Medicine, University of California, Davis, CA 95616

Edited by Michael P. Stryker, University of California, San Francisco, CA, and approved April 30, 2015 (received for review April 1, 2015)

Current models of retinogeniculate development have proposed that connectivity between the retina and the dorsal lateral geniculate nucleus (dLGN) is established by gradients of axon guidance molecules, to allow initial coarse connections, and by competitive Hebbian-like processes, to drive eye-specific segregation and refine retinotopy. Here we show that when intereye competition is eliminated by monocular enucleation, blocking cholinergic stage II retinal waves disrupts the intraeye competition-mediated expansion of the retinogeniculate projection and results in the permanent disorganization of its laminae. This disruption of stage II retinal waves also causes long-term impacts on receptive field size and fine-scale retinotopy in the dLGN. Our results reveal a novel role for stage II retinal waves in regulating retinogeniculate afferent terminal targeting by way of intraeye competition, allowing for correct laminar patterning and the even allocation of synaptic territory. These findings should contribute to answering questions regarding the role of neural activity in guiding the establishment of neural circuits.

retinal waves | retinogeniculate | axon–axon competition | receptive fields | retinotopy

The brain employs several strategies to guide the establishment of correct neural connectivity (1, 2). It has been well recognized that the high specificity of connections between the retina and the dorsal lateral geniculate nucleus (dLGN) is established through several factors. These include gradients of axon guidance molecules that guide the initial coarse targeting of afferent terminals (3–6), and spontaneous retinal activity (retinal waves) that drives competitive processes important for the refinement and segregation of afferent terminal branches (2, 7–15).

Retinal waves are spontaneous propagating bursts of correlated retinal ganglion cell (RGC) activity and have been classified into three developmental stages (1, 15). Stage II retinal waves (from here on also referred to as retinal waves) are extensively studied and have been found to be critical for the development of retinofugal pathways (1, 2, 15). They are mediated by cholinergic signaling from starburst amacrine cells onto RGCs (8, 13, 16–18) and have been hypothesized to drive the Hebbian-like remodeling of RGC afferent terminals (19, 20). Retinal waves play crucial roles in both the establishment of eye-specific segregation (8, 12, 14, 20, 21), through the removal of afferent branches from opposing putative eye-specific domains, and the refinement of afferent terminals within eye-specific laminae, which is believed to be necessary for the establishment of fine-scale retinotopy (12, 22). However, studies have suggested that retinal waves might play additional roles in the development of the retinogeniculate pathway. When retinal waves are blocked during early development, mature lamination in the adult is abnormal (23–25), while eye-specific segregation recovers (26, 27). These results uncovered a retinal wave-dependent window for the development of retinogeniculate lamination. However, the question remains open as to whether these lamination defects are due to abnormal late eye-specific segregation or the disruption of some form of retinal wave-dependent afferent terminal targeting.

A potential retinal wave-dependent mechanism that could regulate retinogeniculate afferent terminal targeting is axon–axon competition originating from the same eye (i.e., intraeye competition). Classic studies in goldfish first demonstrated the principle of axon–axon competition at the optic tectum (28). These studies showed that RGC afferent terminals can undergo expansive or compressive rearrangements in their targeting in response to changes in afferent number, or retinorecipient target size, while maintaining correct retinotopy (28–32). Similarly, neonatal monocular enucleation in ferrets results in an expanded ipsilateral and contralateral projection by adulthood, while correct laminar organization is maintained (7, 10). This demonstrates that retinogeniculate afferent terminals can undergo an expansive and orderly rearrangement due to intraeye competition, and that intereye competition is not required for the establishment of proper retinogeniculate lamination.

To investigate whether retinal waves play a role in regulating retinogeniculate afferent terminal targeting by way of intraeye competition, we monocularly enucleated ferrets one day after birth (P1), to eliminate intereye competition, while also pharmacologically blocking retinal waves (P1– P10) in the surviving eye with the cholinergic agonist epibatidine (EPI) (8, 13, 18). Effects on the targeting of retinogeniculate afferents terminals were assessed anatomically, to characterize impacts on retinogeniculate lamination, and functionally, to assess changes in receptive field (RF) structure and retinotopy in the dLGN. Our results demonstrate that retinal waves regulate afferent terminal targeting by way of intraeye competition during the development of the retinogeniculate pathway.

Results

Retinal Waves Are Critical for the Expansion and Lamination of the Ipsilateral Projection in Enucleates at P10. Neonatal ferrets were monocularly enucleated at P1 to investigate whether the removal

Significance

Spontaneous neural activity is known to play a role in the maturation of nascent neural circuitry. Here we show for the first time a role for early spontaneous correlated retinal activity (i.e., retinal waves) in regulating the laminar targeting and functional development of the retinogeniculate pathway in the monocular condition—a condition where intereye competition and eye-specific segregation are not present. These findings demonstrate the importance of intraeye competition in early visual pathway circuit development. Our results provide a revision to the model of retinogeniculate development and to our general understanding of how neural activity guides the establishment of proper connectivity in the developing brain.

Author contributions: S.F., B.C., and H.-J.C. designed research; S.F. performed research; S.F. analyzed data; and S.F. and H.-J.C. wrote the paper.

The authors declare no conflict of interest.

This article is a PNAS Direct Submission.

[1]Present address: Institute of Neurology, University College London, London WC1N 3BG, United Kingdom, and Institute of Ophthalmology, University College London, London EC1V 9EL, United Kingdom.

[2]Deceased February 11, 2013.

[3]To whom correspondence should be addressed. Email: hjcheng@ucdavis.edu.

This article contains supporting information online at www.pnas.org/lookup/suppl/doi:10.1073/pnas.1506458112/-/DCSupplemental.

of intereye competition would reveal an early intraeye competition-mediated expansion of the ipsilateral projection. Consistent with what has been previously reported in adult enucleates (7, 10), neonatal monocular enucleation resulted in an expansion of the ipsilateral projection by P10, while laminar organization was preserved (23–25) (Fig. 1 *A* and *B*; binocular saline, 0.115 ± 0.004 mm^2; monocular saline, 0.304 ± 0.019 mm^2; $P < 0.0001$). This demonstrated an early intraeye competition-mediated orderly rearrangement of retinogeniculate afferent terminals following enucleation.

If retinal waves regulate afferent terminal targeting by way of intraeye competition, blocking them in enucleates should result in disruptions in ipsilateral lamination. As predicted, the blockade of retinal waves from P1 to P10 prevented the correct lamination of the ipsilateral projection in enucleates, with no identifiable A1 or C1 lamina (23–25) found at P10 (Fig. 1*A*, *Lower Right*). The distribution of afferent terminals was clearly impacted with the blockade of retinal waves, as evidenced by regions of heterogeneous tracer fluorescence intensity (Fig. 1*A*, arrows). Also found

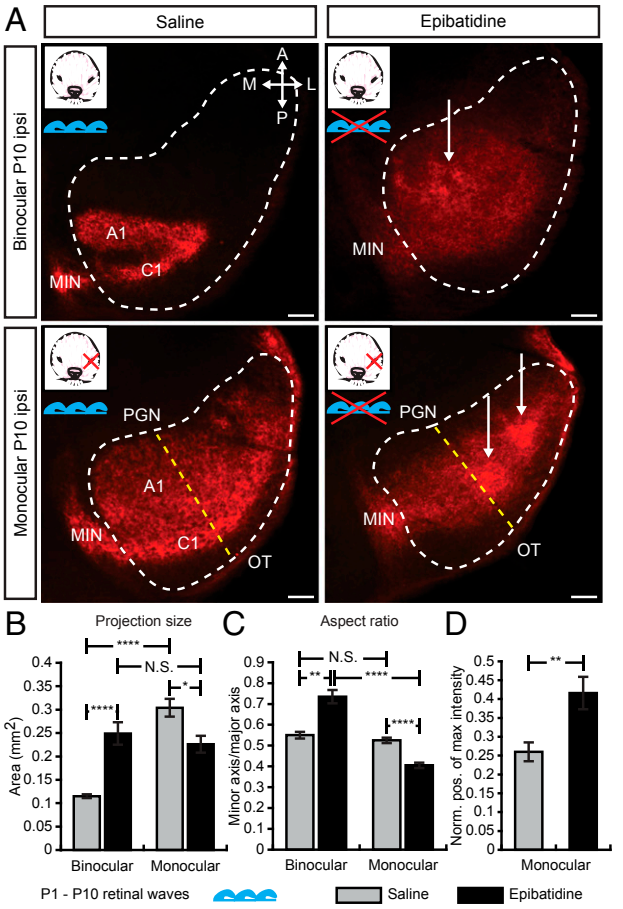

Fig. 1. Blockade of stage II retinal waves disrupts lamination, size, and distribution of ipsilateral projection at P10. (*A*) Ipsilateral retinogeniculate projections shown in the horizontal plane at P10 taken from central dLGN. A1 and C1 laminae, medial interlaminar nucleus (MIN), perigeniculate nucleus (PGN), and optic tract (OT) are labeled. Arrows highlight patches of uneven tracer fluorescence. (*B* and *C*) Plots of the mean projection size (*B*) and aspect ratio (*C*) per condition. (*D*) Plot of the mean normalized position (starting at OT and ending at PGN) of maximum tracer intensity. Intensities were quantified along paths exemplified by dashed lines in monocular ipsilateral images as shown in *A*, *Bottom* (binocular saline, n = five ferrets; binocular EPI, n = five ferrets; monocular saline, n = eight ferrets; monocular EPI, n = nine ferrets; ****$P < 0.0001$; ***$P < 0.001$; **$P < 0.01$; *$P < 0.05$; error bars are SEM). (Scale bar, 100 μm.)

was a shift in afferent terminal concentration orthogonal to the length of the ipsilateral projection (Fig. 1*D*; monocular saline, 0.260 ± 0.025; monocular EPI, 0.416 ± 0.043; $P < 0.01$), consistent with a disruption in laminar targeting.

Most importantly, the size of the ipsilateral projection in enucleates with retinal wave blockade was smaller than in controls at P10, demonstrating a disruption of the intraeye competition-mediated expansion of the ipsilateral projection (Fig. 1*B*; monocular saline, 0.304 ± 0.019 mm^2; monocular EPI, 0.226 ± 0.018 mm^2; $P < 0.05$). This effect is in sharp contrast to what was seen in the binocular condition, where retinal wave blockade resulted in a greatly expanded ipsilateral projection (8, 21, 33) (Fig. 1*B*; binocular saline, 0.115 ± 0.004 mm^2; binocular EPI, 0.249 ± 0.024 mm^2; $P < 0.0001$). In fact, with retinal wave blockade, the size of the ipsilateral projection in monocular and binocular condition did not significantly differ (Fig. 1*B*; monocular EPI, 0.226 ± 0.018 mm^2; binocular EPI, 0.249 ± 0.024 mm^2; $P = 0.867$). Also, following EPI treatment, no change in the size of the dLGN itself was found (saline, 0.407 ± 0.023 mm^2; EPI 0.383 ± 0.008 mm^2; $P = 0.358$). These results suggest that retinal wave-dependent intraeye and intereye competition together shape the size and patterning of the ipsilateral projection (see *Discussion*).

However, surprisingly, we found that some effects on the ipsilateral projection are still dependent on contralateral innervation. Following retinal wave blockade, the aspect ratio of the ipsilateral projection is increased in binocular ferrets (Fig. 1*C*; binocular saline, 0.550 ± 0.016; binocular EPI, 0.735 ± 0.032; $P < 0.01$) but decreased in monocular ferrets (Fig. 1*C*; monocular saline, 0.525 ± 0.013; monocular EPI, 0.405 ± 0.013; $P < 0.0001$). In line with this finding, with the blockade of retinal waves, the aspect ratio was significantly different between monocular and binocular ferrets (Fig. 1*C*; binocular EPI, 0.735 ± 0.032; monocular EPI, 0.405 ± 0.013; $P < 0.0001$) but was not significantly different between monocular and binocular control ferrets (Fig. 1*C*; binocular saline, 0.550 ± 0.016; monocular saline, 0.525 ± 0.013; $P = 0.626$). These results demonstrate that when intereye competition is disrupted in binocular ferrets, ipsilaterally projecting afferent terminals will preferentially target the medial dLGN, which corresponds to the contralateral A lamina (23–25).

Blocking Retinal Waves Results in Abnormal Mature Ipsilateral Retinogeniculate Lamination in Enucleates at P25. We next investigated how blocking stage II retinal waves impacted ipsilateral lamination at P25, following a period of normal retinogeniculate development coinciding with stage III glutamatergic retinal waves (1, 26). As has been previously reported (26, 27), blocking stage II retinal waves in binocular ferrets resulted in fragmentation of the ipsilateral projection at P25 (Fig. 2 *A* and *C*; binocular saline, 23.787 ± 3.622 patches/mm^2; binocular EPI 75.283 ± 7.689 patches/mm^2; $P < 0.001$). P25 enucleates whose stage II retinal waves were blocked also had highly fragmented ipsilateral projections (Fig. 2 *A* and *C*; monocular saline, 19.603 ± 2.928 patches/mm^2; monocular EPI, 68.604 ± 8.758 patches/mm^2; $P < 0.001$), and the magnitude of this effect was no different than that found in binocular ferrets (Fig. 2 *A* and *C*; monocular EPI, 68.604 ± 8.758 patches/mm^2; binocular EPI, 75.283 ± 7.689 patches/mm^2; $P = 0.837$). Similarly, the level of fragmentation, or lack thereof, was the same in both binocular and monocular control ferrets (Fig. 2 *A* and *C*; binocular saline, 23.787 ± 3.622 patches/mm^2; monocular saline, 19.603 ± 2.928 patches/mm^2; $P = 0.777$). These results demonstrate that fragmentation effects are not dependent on disruptions in intereye competition or eye-specific segregation, and thus are likely to be exclusively the result of disruptions in intraeye competition in both monocular and binocular ferrets.

Consistent with what was seen at P10, blocking stage II retinal waves reduced the size of the ipsilateral projection at P25 in both

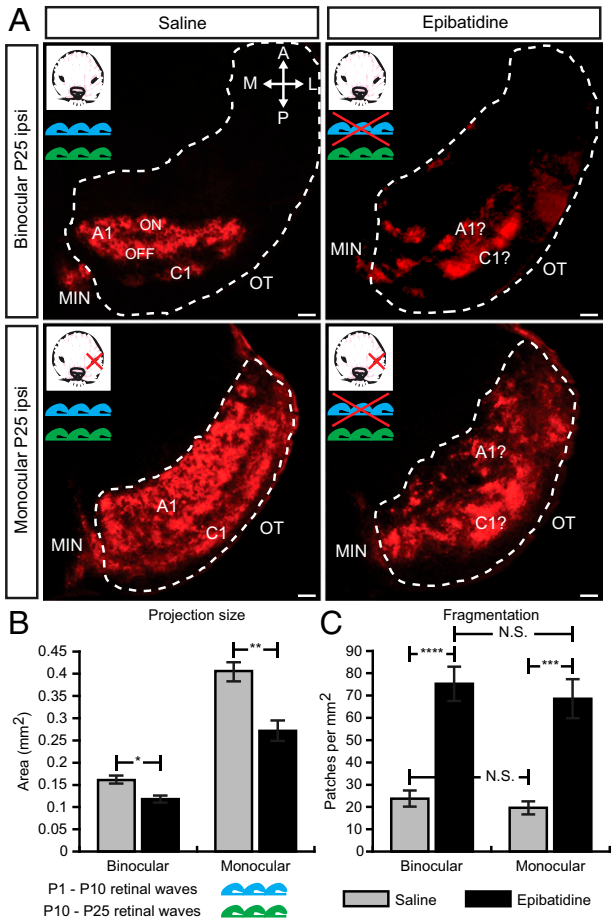

Fig. 2. Blockade of stage II retinal waves reduces and fragments the ipsilateral projection at P25. (*A*) Ipsilateral retinogeniculate projections shown in the horizontal plane at P25 taken from central dLGN. A1 and C1 laminae, ON/OFF sublaminae, medial interlaminar nucleus (MIN), and optic tract (OT) are labeled. (*B* and *C*) Plots of the mean projection size (*B*) and fragmentation level (*C*) per condition (binocular saline, n = five ferrets; binocular EPI, n = five ferrets; monocular saline, n = seven ferrets; monocular EPI, n = nine ferrets; error bars are SEM). (Scale bar, 100 μm.)

monocular (Fig. 2*B*; monocular saline, 0.406 ± 0.020 mm^2; monocular EPI, 0.272 ± 0.023 mm^2; $P < 0.001$) and binocular ferrets (Fig. 2*B*; binocular saline, 0.161 ± 0.010; binocular EPI, 0.118 ± 0.008 mm^2; $P < 0.05$), further demonstrating the importance of stage II retinal waves in the even distribution of afferent terminals across the dLGN by way of intraeye competition.

Retinal Waves Are Critical for the Intraeye Competition-Mediated Expansion of the Contralateral Projection and the Development of Mature ON/OFF Sublaminae in Enucleates. To further investigate the impact of retinal wave blockade on intraeye competition, we quantified effects on the contralateral projection at P10 and P25. Because the contralateral projection is dominated by intraeye competition in both the monocular and binocular condition (i.e., the majority of terminals originate from the same eye), we expected that blocking retinal waves would decrease the size of the contralateral projection in both conditions. As predicted, at P10 following retinal wave blockade, the contralateral projection was affected in both the monocular and binocular condition (Fig. 3). In the binocular condition, there was no significant change in area, despite the filling in of the putative A1 lamina (Fig. 3*B*; binocular saline, 0.546 ± 0.017 mm^2; binocular EPI, 0.558 ± 0.016 mm^2; $P = 0.638$), indicating a decrease in the extent of the projection. For the monocular condition, there was a significant decrease in total area (Fig. 3*B*; monocular saline, 0.519 ± 0.028 mm^2; monocular EPI, 0.399 ± 0.013 mm^2; $P < 0.01$). Interestingly, following retinal wave blockade, we found that there was a consistent lack of afferent terminals in the posterior and medial regions of the dLGN (Fig. 3*A*, asterisks). Consistent with what we described for the ipsilateral projection above, the distribution of afferent terminals was also shifted medially in enucleates, demonstrating a widening of the C lamina (Fig. 3*D*; monocular saline, 0.162 ± 0.017; monocular EPI, 0.366 ± 0.028; $P < 0.001$). However, despite this widening, the ratio of the A and C lamina sizes was unchanged (Fig. 3*C*; monocular saline, 0.874 ± 0.024; monocular EPI, 0.940 ± 0.025; $P = 0.081$).

It has been previously reported that following retinal wave blockade in the binocular condition, ON/OFF sublaminae are unidentifiable (26). However, it was unclear as to whether these effects on sublamination were the result of abnormally late eye-specific segregation or disrupted early afferent terminal targeting. We investigated effects on lamination at P25 in enucleates

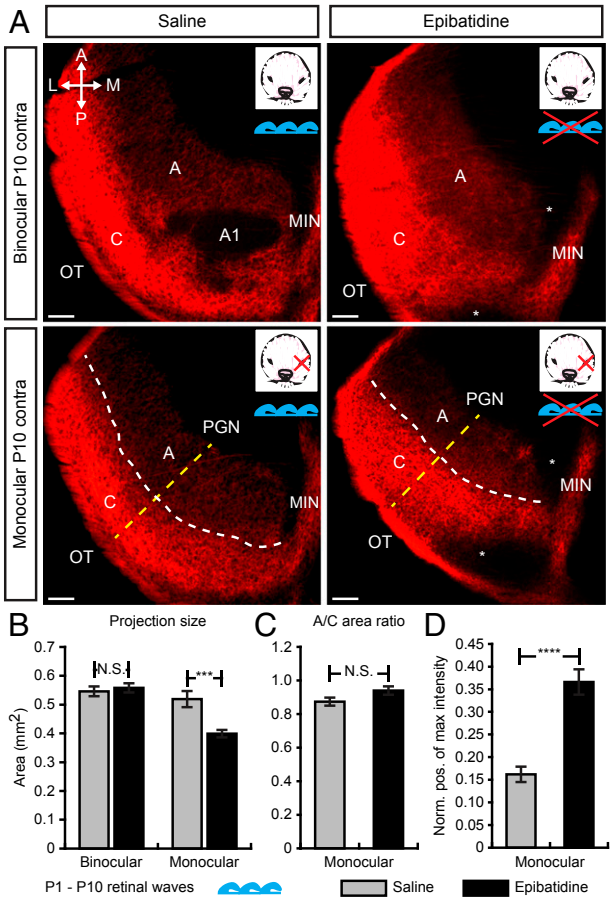

Fig. 3. Blockade of stage II retinal waves disrupts size and distribution of contralateral projection at P10. (*A*) Contralateral retinogeniculate projections shown in the horizontal plane at P10 taken from central dLGN. A and C laminae, A1 lamina, medial interlaminar nucleus (MIN), perigeniculate nucleus (PGN), and optic tract (OT) are labeled. Dashed white line indicates the border between laminae A and C. (*B* and *C*) Plots of the mean projection size (*B*) and A/C lamina area ratio (*C*) per condition (binocular saline, n = 5 ferrets; binocular EPI, n = five ferrets; monocular saline, n = eight ferrets; monocular EPI, n = nine ferrets; error bars are SEM). (*D*) Plot of the mean normalized position (starting at OT and ending at PGN) of maximum tracer intensity. Intensities were quantified along paths exemplified by dashed lines in monocular contralateral images as shown in *A*, *Bottom* (monocular saline, n = 7, monocular EPI, n = 4; error bars are SEM). (Scale bar, 100 μm.)

following retinal wave blockade and discovered that even when eye-specific segregation is absent, ON/OFF sublamination is disrupted as found in the binocular condition (26) (Fig. 4*A*). Interestingly, unlike for the ipsilateral projection, the contralateral projection recovered in size by P25 in both binocular (Fig. 4*B*; binocular saline, 0.928 ± 0.038 mm^2; binocular EPI, 0.866 ± 0.020 mm^2; $P = 0.210$) and monocular ferrets (Fig. 4*B*; monocular saline, 0.812 ± 0.038 mm^2; monocular EPI, 0.800 ± 0.022 mm^2; $P = 0.752$). However, with retinal wave blockade, we found that at P25, the A lamina and C-type laminae became more equal in size, as the ratio of their areas became closer to 1 (Fig. 4*C*; monocular saline, 1.264 ± 0.073; monocular EPI, 1.064 ± 0.025; $P < 0.05$). These results further illustrate the retinal wave-dependent nature of intraeye competition and its role in retinogeniculate afferent termina targeting.

Retinal Wave Blockade Can Disrupt Intraeye Competition Before P10. We have unveiled a role for retinal waves in driving intraeye competition and thus regulating afferent terminal targeting in the retinogeniculate pathway independent of intereye competition and eye-specific segregation. However, the question remained as to whether effects observed at P10 following retinal wave blockade are due to preventing the initial expansion of afferent terminals across the dLGN, or if blockade results in a collapse of expansion and a clustering of terminals. To address this question, we examined the retinogeniculate projection in P5 enucleates after EPI treatment between P1 and P4.

We were surprised to find that in P5 control enucleates, the ipsilateral projection had already reached a size that was observed at P10 (Fig. S1*A*; monocular saline P5, 0.313 ± 0.015 mm^2; monocular saline P10, 0.304 ± 0.019 mm^2; $P = 0.724$). In P5 enucleates whose retinal waves were blocked, ipsilateral lamination and projection size were also relatively normal (Fig. S1 *A* and *B*; monocular saline P5, 0.313 ± 0.015 mm^2; monocular EPI P5, 0.292 ± 0.021 mm^2; $P = 0.455$). This result suggests that blocking retinal waves between P1 and P4 does not completely prevent the initial expansive spread of terminals but that the effects seen at P10 are due to a cumulative disruption in intraeye competition that ultimately results in the abnormal clustering of terminals. However, when the size of the contralateral projection was quantified following retinal wave blockade, we found that, by P5, it was already reduced (Fig. S1 *A* and *B*; monocular saline P5, 0.514 ± 0.028 mm^2; monocular EPI P5, 0.433 ± 0.024 mm^2; $P < 0.05$) and was the same size as that observed at P10 (Fig. S1 *A* and *B*; monocular EPI P5, 0.433 ± 0.024 mm^2; monocular EPI P10, 0.399 ± 0.012 mm^2; $P = 0.289$). This demonstrated that the contralateral projection is susceptible to the effects of retinal wave blockade earlier than the ipsilateral projection. Taken together, these data suggest that the role of retinal wave-dependent intraeye competition is to prevent the abnormal clustering of afferent terminals early in development, and that blocking retinal waves can disrupt intraeye competition by P5.

To verify that all of the effects on the retinogeniculate projection described above were not due to RGC death resulting from early intraocular EPI injections (P1–P10), whole mount retinas were stained for the RGC marker NeuN (34). No changes in RGC density were observed at P25 following intraocular EPI injections (Fig. S2 *A* and *B*; saline, 1,694 ± 89 nuclei/mm^2; EPI, 1,549 ± 65 nuclei/mm^2; $P = 0.1979$) and RGC densities were consistent with that previously reported for ferrets at this age (35).

Blocking Retinal Waves Results in the Enlargement of Ipsilateral Geniculate RFs in Adult Enucleates. There is strong anatomical evidence that retinal waves regulate ipsilateral retinogeniculate afferent terminal targeting by way of intraeye competition. However, understanding the functional consequences of blocking retinal waves could further substantiate the nature of afferent terminal targeting defects. To characterize the functional consequences of retinogeniculate afferent terminal targeting defects on dLGN function, we electrophysiologically recorded visually evoked activity from ipsilateral dLGN cells in adult enucleates (P120+). Using a white noise stimulus to map out RF structure (26, 36–38), we found that adult enucleates, whose retinal waves were blocked, had RF centers that were ∼191% of the size found in controls (Fig. 5*C*; saline 1.531 ± 0.262 visual degrees^2; EPI, 2.929 ± 0.254 visual degrees^2; $P < 0.05$), supporting an abnormal functional convergence of RGC inputs onto dLGN cells. In addition, following the blockade of retinal waves, we found that RF center size varied greatly between neighboring dLGN cells, and was ∼184% of the average difference found in controls (Fig. 5*D*; saline, 0.695 ± 0.073 visual degrees^2; EPI, 1.275 ± 0.121 visual degrees^2; $P < 0.0001$). This large difference in RF center size between adjacent dLGN cells supports a heterogeneous convergence of retinogeniculate inputs following retinal wave blockade, consistent with observed anatomical abnormalities in mature ipsilateral retinogeniculate afferent terminal targeting and clustering (Figs. 1 and 2). Interestingly, previous studies in mice have associated retinal waves with enlargements in RF size in retinofugal targets, but exclusively along the azimuth axis (6, 39). We find, however, that changes in RF size were symmetric, as there were no changes in the RF aspect ratio following

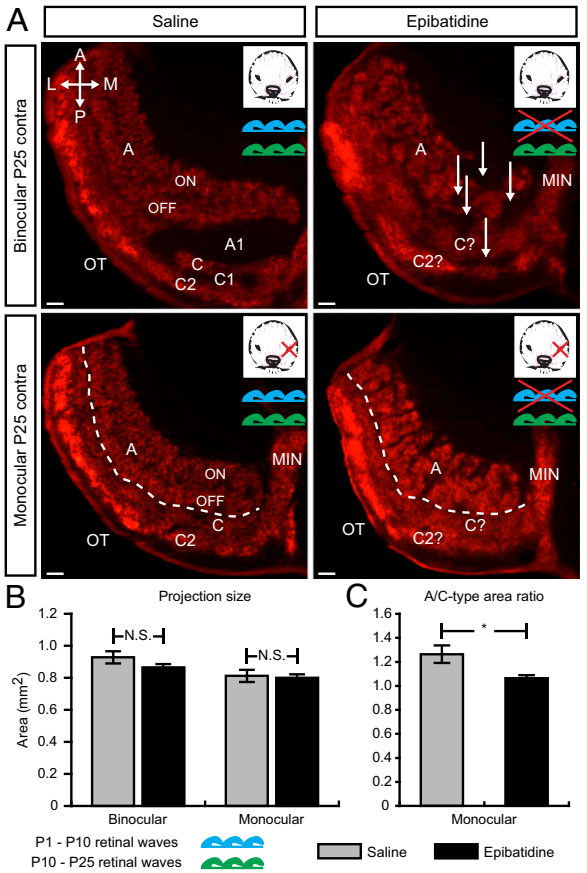

Fig. 4. Blockade of stage II retinal waves disrupts the mature lamination of the contralateral projection at P25. (*A*) Contralateral retinogeniculate projections shown in the horizontal plane at P25 taken from central dLGN. A and C/C2 contralateral laminae, A1 and C1 ipsilateral laminae, ON/OFF sublaminae, medial interlaminar nucleus (MIN), and optic tract (OT) are labeled. Arrows indicate the fragments of the ipsilateral projection following retinal wave blockade. White dashed line indicates the border between the A lamina and C-type laminae. (*B* and *C*) Plots of the mean projection size (*B*) and A/C-type (C and C2 combined) laminae area ratio (*C*) per condition (binocular saline, n = five ferrets; binocular EPI, n = five ferrets; monocular saline, n = seven ferrets; monocular EPI, n = nine ferrets; error bars are SEM). (Scale bar, 100 μm.)

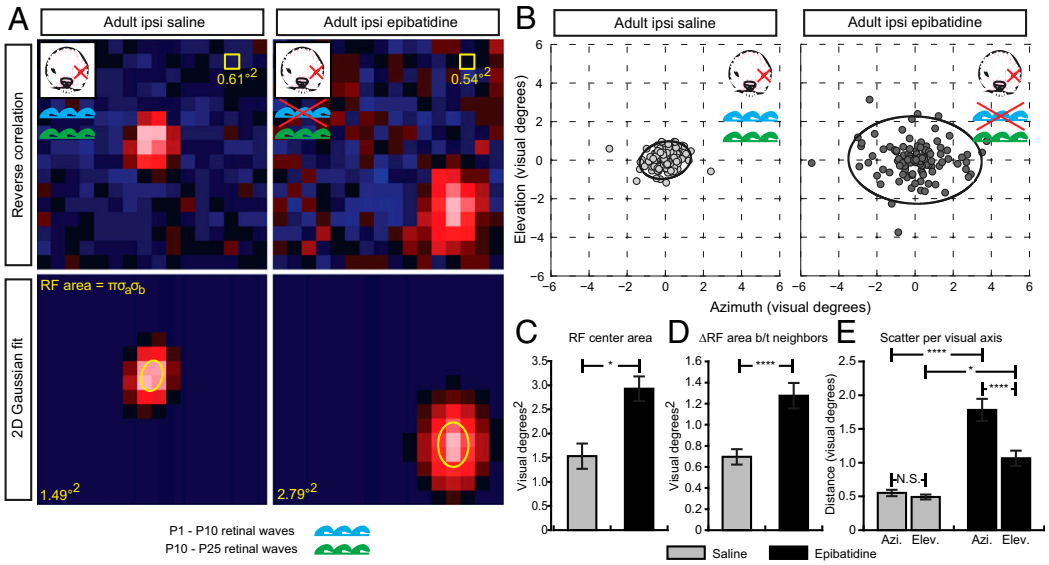

Fig. 5. Blockade of stage II retinal waves enlarges and retinotopically misaligns RFs of ipsilateral (ipsi) dLGN cells in adult (P120+) enucleates. (*A, Top*) Examples of adult (P120+) ipsilateral dLGN cell RFs mapped using reverse correlation analysis. Red pixels correspond to ON regions, and blue pixels correspond to OFF regions (i.e., regions of the RF that respond to increments of light or decrements of light). Yellow box indicates scaling. (*Bottom*) Bivariate Gaussian fits to RF centers. For each example, the RF center area is designated by the yellow ellipse, and its area is shown in the lower left corner. (*B*) Scatter plot of the mean centered RF locations for all simultaneously recorded groups of two or more dLGN cells for both conditions. Orientation and length of elliptical axes represent the two SDs along axes of the principle components of the data, to visualize directions of maximum variance. (*C*) Plot of the mean RF center area following saline or EPI treatment (saline, $n = 198$ cells, three ferrets; EPI, $n = 136$ cells, three ferrets). (*D*) Plot of the mean difference in RF area between simultaneously recorded dLGN cells. (*E*) Plot showing the mean distances between the RF locations of simultaneously recorded dLGN cells, along azimuth and elevation axes of visual space (saline, $n = 187$ cells, three ferrets; EPI, $n = 108$ cells, three ferrets; error bars are SEM).

retinal wave blockade (saline, 1.064 ± 0.036; EPI, 1.023 ± 0.037; $P = 0.807$).

As has been previously reported in adult binocular ferrets following retinal wave blockade (26), there were no effects on ON and OFF cell composition or segregation in enucleates (Fig. 6 *B* and *C*). No difference in the percentage of ON or OFF cells whose RFs were mapped was found (Fig. 6*B*; saline ON percentage, 84.734 ± 13.822; EPI ON percentage, 93.782 ± 2.813; saline OFF percentage, 15.266 ± 13.822; EPI OFF percentage, 6.217 ± 2.813; $P = 0.582$). Additionally, the percentage of neighboring cell pairs that were the same sign (ON or OFF) was also unchanged (Fig. 6*C*; saline, 0.959 ± 0.033; EPI, 0.946 ± 0.027; $P = 0.768$), showing that cells were equally segregated by sign in both conditions.

Blocking Retinal Waves Disrupts Ipsilateral dLGN Fine-Scale Retinotopy in Adult Enucleates. We next investigated the impact of blocking retinal waves on the development of ipsilateral retinotopy in adult enucleates, as one might expect abnormal retinotopy would be associated with fragmented ipsilateral lamination (Fig. 2). Effects on fine-scale retinotopy were investigated on both a local and widespread scale in the dLGN. First, we quantified the retinotopic alignment of RFs of adjacent dLGN cells, recorded simultaneously with a multiunit electrode. In controls, RF locations of adjacent dLGN cells were tightly aligned in visual space, with no difference in retinotopic alignment found between azimuth and elevation axes (Fig. 5 *B* and *E*; saline azimuth, 0.551 ± 0.047 visual degrees; saline elevation, 0.492 ± 0.036 visual degrees; $P = 0.939$). Enucleates whose retinal waves were blocked showed a disruption of retinotopic alignment (i.e., an increase in the scatter of RF locations of simultaneously recorded cells) along both the azimuth axis (Fig. 5 *B* and *E*; saline, 0.551 ± 0.047 visual degrees; EPI, 1.782 ± 0.164 visual degrees; $P < 0.0001$) and the elevation axis (Fig. 5 *B* and *E*; saline, 0.492 ± 0.036 visual degrees; EPI, 1.065 ± 0.113 visual degrees; $P < 0.05$) of visual space, with the largest effect on retinotopic alignment found along the azimuth (Fig. 5 *B* and *E*; EPI azimuth, 1.782 ± 0.164 visual degrees; EPI elevation, 1.065 ± 0.113 visual degrees; $P < 0.0001$).

Additionally, we investigated changes in fine-scale retinotopy along the length of a single electrode penetration tract (40). In controls, changes in electrode depth had a strong relationship with shifts in RF location along both the azimuth and elevation axis of visual space (Fig. 7 *B* and *C*; saline, Δelectrode depth vs. Δazimuth, $P < 0.0001$; Δelectrode depth vs. Δelevation, $P < 0.0001$). However, when retinal waves were blocked, the relationship between change in electrode depth and change in RF location along the azimuth axis was abolished (Fig. 7*B*; EPI, Δelectrode depth vs. Δazimuth, correlation not significant, $P = 0.223$). This effect was significant compared with controls (Fig. 7*B*; Δelectrode depth vs. Δazimuth, saline vs. EPI, $P < 0.0001$), indicating a severe disruption of azimuth fine-scale retinotopy. With retinal wave blockade, a relationship was preserved between change in electrode depth and change in RF location along the elevation axis (Fig. 7*C*; EPI, Δelectrode depth vs. Δelevation, $P < 0.0001$). However, the blockade of retinal waves still resulted in a significant disruption in fine-scale retinotopy along the elevation axis (Fig. 7*B*; Δelectrode depth vs. Δelevation, saline vs. EPI, $P < 0.01$). These results indicate that retinal waves are critical for the development of fine-scale retinotopy along both axes of visual space, and these disruptions are correlated with lamination and afferent terminal targeting defects in enucleates.

Finally, given the significant functional changes in adult enucleates following retinal wave blockade, we examined effects on adult retinogeniculate lamination. In adult enucleates following retinal wave blockade, we found that the ipsilateral A1 and C1 laminae appeared abnormal and less contiguous, with the contralateral projection showing abnormal ON/OFF sublamination (Fig. 6*A*). Additionally, we measured the height of the putative A1 lamina in adult enucleates whose dLGNs were recorded from for RF mapping experiments. From these recordings, we found that the electrode run length was significantly shorter in enucleates whose retinal waves were blocked, suggesting that their retinogeniculate laminae

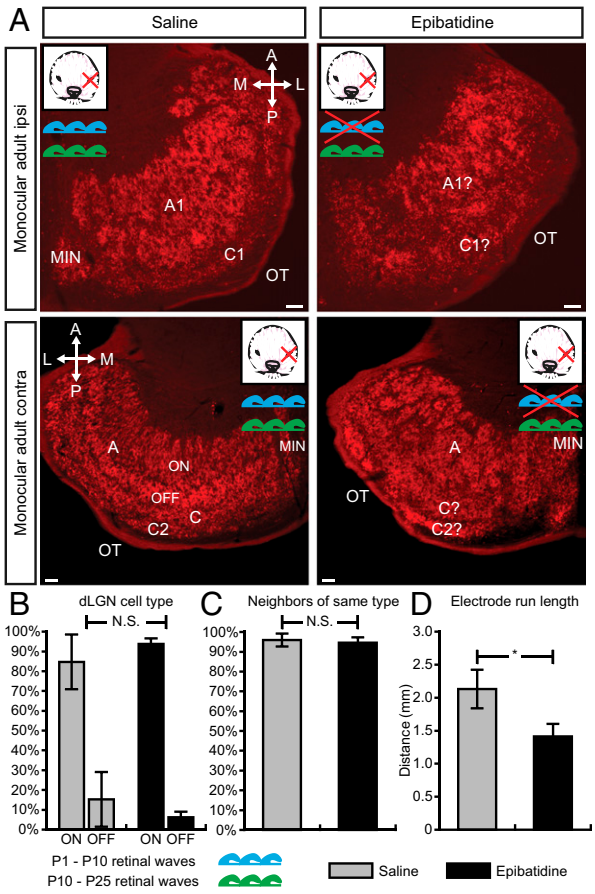

Fig. 6. Effects of stage II retinal wave blockade on adult anatomy and ON/OFF segregation. (*A*) Ipsilateral and contralateral retinogeniculate projections shown in the horizontal plane at adulthood taken from central dLGN. A and C laminae, A1 and C1 laminae, medial interlaminar nucleus (MIN), and optic tract (OT) are labeled. (Scale bar, 100 μm.) (*B*) Plot of the mean percentage of geniculate cell types found in putative A1 lamina of saline and EPI treated ferrets. (*C*) Plot of the mean percentage of neighboring geniculate cells recorded simultaneously that are of the same sign (ON–ON or OFF–OFF; saline, n = three ferrets; EPI, n = three ferrets; error bars are SEM). (*D*) Plot of the mean electrode run length through the putative A1 region in saline and EPI treated ferrets (saline $n = 9$, three ferrets; EPI, $n = 9$, three ferrets; error bars are SEM).

were abnormally smaller in size (Fig. 6*D*; saline, 2.131 ± 0.292 mm; EPI, 1.413 ± 0.190 mm; $P < 0.05$). Together, the anatomical and functional data from the adult enucleates demonstrate that retinal waves are critical for the establishment of retinogeniculate circuitry during visual system development.

Discussion

Using monocular enucleates to completely eliminate the influences of intereye axon–axon competition, we have uncovered a critical role for stage II retinal waves in driving intraeye axon–axon competition, which is required for normal retinogeniculate afferent terminal targeting. This conclusion is supported by the various anatomical and physiological effects of retinal wave blockade on the ipsilateral and contralateral projection, from P10 to adulthood.

The effects on the ipsilateral projection, following the blockade of retinal waves, present a strong case for a generalization of the mechanisms underlying early intraeye and intereye competition, as the effects seen in the monocular and binocular condition demonstrate complementary roles for intereye and intraeye axon–axon competition in mediating laminar patterning (Fig. S3). In the case of the binocular condition, the ipsilateral projection fails to undergo compression mediated mainly by intereye competition with numerically dominant contralateral afferents. Conversely, in the case of the monocular condition, where contralateral afferents have been removed, the ipsilateral projection fails to maintain the expansion mediated by ipsilateral intraeye competition (Fig. 1 *A* and *B* and Fig. S3). Decreases in the size of the contralateral projection are seen in both monocular and binocular ferrets following retinal wave blockade, and are consistent with disruptions in intraeye competition that are dominant in both conditions (Fig. 3*A*).

What neurobiological mechanism underlies the retinal wave-dependent expansion seen in enucleates? Although a Hebbian-

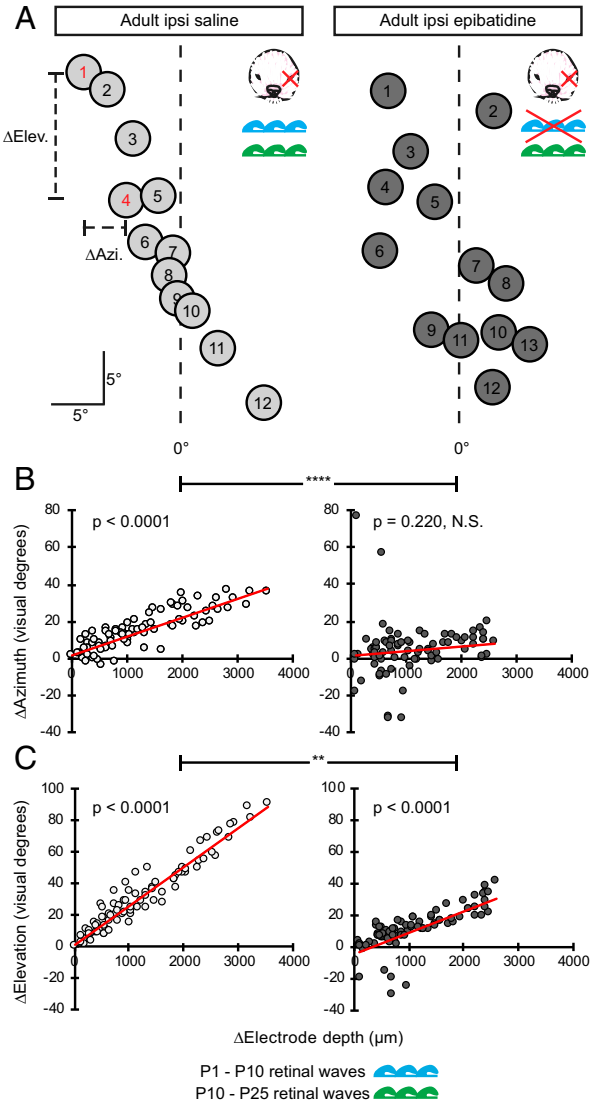

Fig. 7. Ipsilateral fine-scale retinotopy is disrupted in enucleates following stage II retinal wave blockade. (*A*) Illustration of locations of ipsilateral RFs for dLGN cells encountered along a single electrode penetration tract in an adult enucleate (P120+). RFs are numbered in the order in which their corresponding cells were encountered by the electrode. Changes in RF location along azimuth and elevation axes, relative to the RF location of the first encountered cell, were determined for each subsequent cell's RF. Scatter plots are shown for change in electrode depth versus change in RF location along the (*B*) azimuth axis or (*C*) elevation axis of visual space, for all dLGN cells. A P value is shown for each condition to indicate the significance of the relationship between change in electrode depth and change in RF location as assessed by a hierarchical linear model. Fit trend lines are in red (saline, $n = 83$ cells, three ferrets; EPI, $n = 82$ cells, three ferrets; error bars are SEM).

like mechanism is thought to drive retinogeniculate afferent terminal refinement (19, 20, 41), its disruption alone is unlikely to explain the failure of the retinogeniculate projection to expand in enucleates following the blockade of retinal waves. For example, previous work has supported a role for retinal waves in the pruning and consolidation, not the expansion, of retinogeniculate afferent terminals early in development (11, 12). Additionally, monocular enucleation has limited effects on afferent terminal morphology in both cats and primates (42, 43), with only afferent terminals from Y RGCs expanding in cats (44). Y-like RGCs do not innervate either the ipsilateral A1 or C1 laminae in ferrets (45), so it is unlikely that the expansion of the ipsilateral projection could be explained by changes in afferent terminal morphology. However, although EPI blocks retinal waves, it has also been shown to increase the firing rates of some RGCs (8, 18), possibly raising the question as to whether the effects on ipsilateral and contralateral projection size could be caused by an acceleration of afferent terminal refinement due to increased total RGC activity. This is also unlikely because, although EPI increases tonic firing rates for some cells, it completely silences many others (8, 18). The EPI also greatly attenuates or eliminates high firing rates during RGC bursting activity, which are thought to be critical for Hebbian-like refinement (18, 20, 41, 46, 47). Additionally, when retinal waves were blocked in mice with EPI, terminal zones (TZs) corresponding to focally labeled retinocollicular afferent terminals were enlarged at P7 (39). If EPI treatment exclusively led to a refinement of RGC afferent terminals, one would expect that TZs in the superior colliculus would decrease in size, not increase. Lastly, recent work has also argued that a presynaptic non-Hebbian mechanism underlies retinogeniculate lamination, showing that when glutamate release by ipsilaterally projecting retinogeniculate afferents is attenuated, thus silencing postsynaptic activity in the dLGN, the patterning and size of the ipsilateral projection is normal (48). All together, these findings support the expansion of the retinogeniculate projection (Fig. 1 *A* and *B*) being mediated primarily by retinal wave-dependent intraeye axon–axon competition and not Hebbian-like afferent terminal refinement.

The fragmentation effects on P25 ipsilateral lamination are likely the direct consequence of abnormal terminal clustering following retinal wave blockade (Figs. 1 and 2). However, they are also reminiscent of effects seen in rodent models where the expression of ephrin-A axon guidance molecules are disrupted (3). This has led some to hypothesize a role for retinal waves in driving the read-out of molecular guidance cues. In vitro work has also supported this possibility, as blocking spontaneous activity in cultured RGCs using tetrodotoxin resulted in their abnormal responses to ephrin-A, although responses were rescued by the cyclic release of cAMP (49), whose intracellular levels are known to be associated with retinal waves (50). However, more recent in vivo work, where RGC afferent terminals innervating the superior colliculus were silenced by ectopic expression of the inward rectifying potassium channel Kir 2.1, demonstrated that retinal activity was not required for afferent responses to ephrin-A (51). This result argues against a role for retinal activity in regulating the readout of molecular guidance cues, and is consistent with retinal wave-dependent effects on retinogeniculate afferent terminal targeting being due to disruptions in axon–axon competition.

One interesting point is that not all effects on retinogeniculate afferent terminal targeting are exclusively retinal wave dependent. When retinal waves are blocked, some aspects of retinogeniculate afferent terminal targeting by P10 are revealed to be dependent on contralateral innervation. Afferent terminals in binocular ferrets target the medial region of the dLGN, where the contralateral A lamina is located (Fig. 1 *A* and *C*). This result is consistent with what has been reported following the silencing of stage III retinal waves, which results in the ipsilateral projection cooccupying the contralateral laminae by P25 (52). Both these previous results and our findings (Fig. 1*C*) suggest that ipsilaterally projecting afferents are attracted to regions of contralateral innervation, although the underlying cause is unknown.

Some notable differences are found when comparing the effects of retinal wave blockade between the ipsilateral and contralateral projection, particularly the effects on sublamination and differences in the timing of effects on, and recovery of, projection size (Figs. 2 and 4 and Fig. S1). Differences in the timing of effects on projection size can likely be attributed to differences in the magnitude of intraeye competition between the ipsilateral and contralateral projection. As the contralateral projection has more afferents originating from the same eye (i.e., more intraeye competition), it may experience accelerated effects due to abnormal or normal retinal activity. This is supported by the early decrease in contralateral projection size at P5 due to retinal wave blockade (Fig. S1 *A* and *B*), and its recovery in size by P25 following the period of normal stage III retinal wave activity after P10 (Fig. 4*A*). Regardless, the contralateral projection still shows permanent effects on ON/OFF sublamination due to retinal wave blockade, indicating limits to its ability to recover from abnormal retinal wave activity (Fig. 6*A*).

With retinal wave blockade, what is the exact relationship between observed anatomical effects and functional abnormalities in the dLGN of enucleates? Previous studies using mouse models of retinal wave disruption were the first, to our knowledge, to demonstrate the importance of early spontaneous retinal activity in refining functional connectivity in the dLGN (6, 22). These experiments proposed a model in which, following retinal wave blockade, afferent terminals would remain improperly pruned, or enlarged, thus resulting in topographic mistargeting (22). This argument was supported by the fact that TZs in the dLGN were enlarged (12, 22). Additionally, work has shown that the morphology of single retinogeniculate axon terminals in mice is initially enlarged when retinal waves are disrupted (11). Interestingly, as shown above, we find that following retinal wave blockade in the enucleated ferret, the total size of the projection is diminished (Figs. 1 and 2 and Fig. S1). This result is important, in that one would expect that if terminal branch pruning was exclusively affected, the total projection size would either increase or stay the same. A decrease in projection size, despite enlarged afferent terminals, ultimately leads to the conclusion that there is an increase in afferent terminal overlap due to disruptions in afferent terminal targeting. Consistent with this expectation, we found that following retinal wave blockade in enucleates, the size of geniculate RFs also increases (Fig. 5*C*), indicating a greater amount in functional convergence.

Surprisingly, despite disruptions in afferent terminal refinement in mouse models of retinal wave blockade (11), geniculate RFs in these animals have been reported to be normal (22). Why is it that when retinal waves are blocked, geniculate RFs are enlarged in adult ferrets (Fig. 5) but not in adult mice (22, 53)? One possibility is that the laminar structure of the ferret dLGN limits the extent of its developmental plasticity (23–25, 54). Because ferret dLGNs have cellular lamination, unlike the mouse, and also express molecules inhibiting neurite outgrowth between laminae (55), it is likely that retinogeniculate plasticity is reduced at more mature time points. The bulk of RF refinement is thought to occur after eye opening in the ferret (37), a time at which abnormal lamination might result in refinement defects. Interestingly, although geniculate RFs have been reported to be normal in β2 KO mice, collicular RFs have been shown to be enlarged (39, 56). This may represent differences in the timing of development and/or long-term plasticity between the dLGN and superior colliculus in the mouse. For example, differences in the time course of refinement have been found between retinogeniculate and retinocollicular afferent terminals, with retinocollicular terminals maturing approximately a week earlier (11).

What anatomical effects underlie disruptions in fine-scale retinotopy in the ferret? As mentioned above, studies on the effects of retinal wave blockade have proposed that disruptions in functional fine-scale retinotopy were exclusively due to a lack of afferent terminal branch pruning, as demonstrated by enlargements in TZ size (22). However, as the TZ labeling approach results in the tracing of many RGCs and not single-axon terminal arbors, this interpretation is not conclusive. Indeed, more recent work studying the effects of retinal wave disruption on single axons in β2 KO mice found that by P14–15, effects on axon arbor size were not significantly different from wild type (11), despite TZ size being enlarged at this age (22). Although we currently do not have conclusive evidence to support this hypothesis, we find it likely that with retinal wave blockade, the observed effects on TZ size and fine-scale retinotopy in mice, and the effects on fine-scale retinotopy in ferrets (Figs. 5 and 7), are not exclusively the result of improper afferent terminal pruning. Another likely explanation is disruptions in retinal wave-dependent axon–axon competition-mediated afferent terminal targeting. Under this model, disrupting axon–axon competition, either intraeye or intereye, would result in functional fine-scale retinotopic mistargeting similar to what we have seen in our experiments (Fig. S3). Future work that can combine the strengths of bulk axon labeling and single-axon tracing, such as Brainbow tools (57), will ultimately be necessary to answer this question.

Taken together, our results and others' support a retinal wave-dependent axon–axon competition-based (intraeye and intereye competition) model for retinogeniculate afferent terminal targeting. This axon–axon competition is necessary for the proper distribution of afferent terminals into stereotyped laminae and their even allotment of synaptic territory in the dLGN (Fig. S3). Axon–axon competition appears to likely be distinct from conventionally understood molecular guidance or Hebbian-like refinement. Our findings regarding the, at times controversial (58, 59), role of retinal waves provide an important revision to the model of retinogeniculate development and to our general understanding of how neural activity guides the establishment of proper connectivity in the developing brain.

Materials and Methods

Animals. Time pregnant ferrets were received at mid to late gestation, giving birth 2–3 wk later (Marshall BioResources). Food and water were provided ad libitum, and ferret offspring were provided with softened food from 2.5 wk of age until fully weaned. All procedures were authorized by the University of California, Davis Institutional Animal Care and Use Committee and performed in accordance with national standards for humane animal research as set forth by the National Institutes of Health, Institute of Laboratory Animal Research, Federation of Animal Science Societies, US Department of Agriculture, Public Health Service, and Assessment and Accreditation of Laboratory Animal Care, International.

Monocular Enucleation. Neonatal ferrets at P1 were deeply anesthetized with isoflurane. Topical lidocaine was applied to the left eye. The eyelids were separated, and the muscles and connective tissue of the eyeball were blunt dissected. Hemostats were used to clamp the optic nerve, after which it was severed and the eyeball removed. Antibiotic ointment was applied to the orbit, and sterile gelfoam was inserted to stem any subsequent bleeding. Liquid suture was applied to seal the eyelids (GLUture; Abbott Laboratories). Before the animal fully awakened, a single dose of buprenex was administered intramuscularly (0.02 mg/kg) as a postoperative analgesic.

Neonatal EPI Injections. Neonatal ferrets were injected with EPI in the right eye every 48 h starting at P1 and ending at P4 for P5 analysis or at P9 for analysis at P10 or after, to block stage II retinal waves as previously described (8, 26, 60). Using a Hamilton syringe, sterile saline with or without 1 mM EPI was intraocularly injected at an initial volume of 1.0 μL, and increased by 0.25 μL every 48 h until reaching a final volume of 2.0 μL for P9 injection.

Labeling Retinogeniculate Afferents. As previously described (25, 26, 38), cholera toxin B (CT-B) subunit conjugated to a red Alexa Fluor dye (CT-B 594; Invitrogen) was injected intraocularly (5 μg/μL) into the right eye at either P4, P9, P24, or P120+ to visualize retinogeniculate afferents for subsequent image analysis. Injection volumes of CT-B were 1.5 μL at P4, 2 μL at P9, 6 μL at P24, and 18 μL at P120+. After 24 h, ferrets were transcardially perfused with saline and then 4% (mass/vol) paraformaldehyde. Brains were removed and postfixed overnight and then cryoprotected in 30% sucrose until sunk. Cryoprotected brains were sectioned parallel to the horizontal axis on a freezing microtome at 40 μm thickness and mounted to slides for imaging.

Quantifying Retinal Ganglion Cell Density. To quantify RGC density, whole retinas were stained for the RGC marker NeuN. Retinas from a subset of monocular and binocular P25 ferrets were removed following transcardial perfusion, as described above, and additionally postfixed for 1 h. Whole retinas were then incubated for 24 h in an anti-NeuN primary antibody (EMD Millipore), washed in PBS for 24 h, incubated in Alexa Fluor 488 secondary antibodies (Invitrogen) for 24 h, and washed an additional 24 h before being mounted. Immunofluorescently stained retinas were flat mounted after four radial relieving cuts were made with equal spacing. Four images were taken at 20× while focused on the ganglion cell layer, one at the midlength of each retinal quadrant. Using the image analysis software Fiji, a distribution of ImageJ (National Institutes of Health) (61), images were background subtracted and autothresholded to segment stained nuclei. To increase the accuracy of cell counting, overlapping nuclei were separated using the watershed function, after which thresholded nuclei were detected and counted using an automated cell counter.

Analysis of Retinogeniculate Projections. Sections containing labeled retinogeniculate afferents were imaged on an epifluorescence microscope under a 5× or 10× objective, depending on the size of the dLGN (typically 10× for P5/P10 and 5× for P25). Micrographs were captured using a CCD digital camera and Axiovision software (Zeiss). All image processing and analyses were carried out in Fiji, a distribution of ImageJ (National Institutes of Health) (61). For each animal, five sections from the middle of the dLGN were used for image analysis. Images of horizontal sections with CT-B-labeled retinogeniculate afferents were converted to grayscale and cropped to the borders of the dLGN. Images were then thresholded to 30% above background. Thresholding resulted in a binary image where white pixels corresponded to retinogeniculate afferents and black pixels to areas lacking any afferent input. The aspect ratio of projections was calculated by autofitting an ellipse to thresholded ipsilateral afferents, excluding pixels corresponding to the medial intralaminar nucleus (MIN) and optic tract (OT). The resulting minor axis was divided by the major axis to calculate the aspect ratio. Similarly, the fragmentation of the ipsilateral projection in a P25 section was quantified by autocounting clusters of pixels (corresponding to projection patches), with a minimum area of 350 μm^2 and no maximum, excluding pixels corresponding to the MIN and OT. A minimum of 350 μm^2 was chosen as it is the reported average size of dLGN neurons (54), and thus helped to eliminate the counting of artifactual pixels. Retinogeniculate projection patches per square millimeter were calculated by summing the area of all pixels included in the patch count analysis, determining the corresponding area those pixels represented based on preset scales (46 pixels = 100 μm with a 5× objective; 92 pixels = 100 μm with a 10× objective), and dividing by the number of patches counted. To quantify the distribution of afferent terminals, by assessing fluorescence across the dLGN, an intensity plot was taken along the center of the projection, orthogonal to its major axis. Intensity plots started at the OT and ended at the perigeniculate nucleus (PGN). The intensity plot analysis was only carried out on images taken at 10×, as this magnification was superior for capturing fluorescent gradients. The length of the intensity plot was normalized for each image quantified, and the position of peak fluorescence intensity was calculated for treatment comparisons. To quantify total dLGN size, borders of the dLGN were determined by the OT, axons of passage, and autofluorescence within sections, which allowed for the identification of the PGN. Measured areas were consistent with those found in sections stained with a fluorescent marker of Nissl.

Extracellular Electrophysiology Recordings of dLGN Cells. As described (26, 38, 60), P120+ monocularly enucleated adult ferrets were initially anesthetized with an intramuscular (IM) injection of a ketamine (40 mg/kg) acepromazine (0.4 mg/kg) mixture. Atropine (0.6 mg) was injected IM to inhibit mucus secretion in the trachea. A catheter was inserted either i.v. or intraperitoneally (IP) for the administration of fluids. After a tracheotomy was performed, the animal was transferred to a modified kitten stereotaxic, where it was placed in ear bars and connected to a respirator. The primary anesthetic was 2–4% isoflurane, and exhaled CO_2 was monitored and maintained at a level between 3.5% and 4%. The animal's heart rate was monitored by EKG, and its

temperature was kept at 37.5 °C. Lactated ringer's solution, with the paralytic vecuronium bromide (0.2 mg/kg), was administered continuously at a rate of 1 mL·h^{-1}·kg^{-1} by way of IV or IP catheter. Atropine and phenylephrine hydrochloride drops were administered to dilate the pupil, after which a plano hard contact lens was placed on the eye. A craniotomy was performed to remove a 4 mm × 4 mm piece of skull centered at stereotaxic coordinates anterior-posterior −1, medial-lateral +5.8. The dura was removed, and warm 3% agar in saline was applied to seal the brain and prevent drying. A lacquered tungsten multiunit electrode (Microprobes) with an impedance of ∼1.5 MΩ was lowered with a microdriver, targeting the dLGN. The electrode penetrated the brain orthogonal to the cortical surface, the site of penetration being based on above stereotaxic coordinates and cortical landmarks. Visual responses were tested every 200 μm starting at a depth of 3,000 μm. Multiple penetrations were made with a spacing of 300 μm until visual responses from the dLGN were detected on an oscilloscope and audio amplifier, after which the electrode was advanced with a spacing of at least 100 μm, but 258 μm on average. The ON/OFF, or OFF/ON, center-surround RF structures of geniculate cells were mapped by reverse correlation using a pseudorandom binary (100% contrast) white noise visual stimulus (m-sequence) as described (36), displayed on a cathode ray tube monitor (Eizo) with a mean luminance of 40–50 candelas per square meter and a refresh rate of 120 Hz. The m-sequence consisted of a 16 × 16 grid of pseudorandomly assigned white and black squares that were updated every one, two, or three frames (8.3 ms, 16.7 ms, and 25 ms respectively). Filtered waveforms were recorded by a CED Power 1401 interface connected to a PC with Spike2 data acquisition and analysis software (Cambridge Electronic Design). Spike sorting was carried out both online by Spike2, to determine RF locations and cell type during experiments, and offline with Offline Sorter (Plexon), by way of PCA analysis, for final data quantification purposes.

Quantification of Receptive Field Area and Fine-Scale Retinotopy. The spatiotemporal structures of RFs were characterized using reverse correlation analysis (36). All mapped RFs used for the analyses described below were found within 25 visual degrees of central gaze. To quantify the area of RF centers, a bivariate Gaussian was fit to the peak of ON or OFF center responses as described (37). The area of an RF center was thus calculated as the area of an ellipse, with the major and minor axes corresponding to the SDs of the major and minor axes of the fit bivariate Gaussian, $RF = \sigma_a \sigma_b \pi$. The comparison of RF center areas between neighboring dLGN cells was made only for cells recorded simultaneously with a multiunit electrode, and isolated by spike sorting as described above. Quantifications of RF alignment were made similarly, by comparing the location of RF centers for simultaneously recorded cells. Characterizations of fine-scale retinotopy along the depth of an electrode penetration tract were assessed by hand-mapping RFs on a tangent screen, using a light gun to probe the edges of RF centers. Cells were isolated for RF hand-mapping by observing oscilloscope displayed spike waveforms. RFs were numbered according to the order in which they were hand-mapped along the length of an electrode penetration. Digital images were taken of the entire tangent screen containing hand-mapped RFs, with a scale bar included for the correct quantification of distance in visual degrees. Tangent screen images were analyzed in Fiji, a distribution of ImageJ (National Institutes of Health) (61). Relative RF center locations were quantified using the point selection tool, following the scaling of the image based on the drawn scale bar. Difference in RF location along the azimuth (*x* axis) and elevation (*y* axis) from the first mapped RF was calculated. Shifts in position along the azimuth and elevation axes of visual space were compared with changes in electrode position that was noted previously with cell isolation and hand-mapping.

Statistical Analysis. Descriptive statistics were reported as mean ± SEM. Significance values for comparisons of anatomical means were calculated using a two-way ANOVA when means were compared between binocular and monocular conditions; otherwise, a Student's *t* test was used. For the statistical analysis of electrophysiological data, where cells recorded from the same ferret would violate assumptions of independence, hierarchical statistical models were used (i.e., a mixed model ANOVA or a hierarchical linear model), or values were averaged per animal and a Student's *t* test was used. Because ANOVA models are robust to failures of normality, assumptions of normality were assumed met unless histograms of residuals showed the distributions to be highly skewed. Assumptions of homoscedasticity were checked visually and with Levene's test. If heteroscedasticity was found using either approach, a weighted least squares procedure was implemented in the case of a two-way ANOVA, and the Satterthwaite method for degrees of freedom was used for hierarchical models. Multiple comparisons were made using the Tukey–Kramer method or Fisher's least significant difference test, where applicable. For fine-scale retinotopy data to determine if early retinal waves disrupted the relationship between change in electrode position and change in RF location, a hierarchical linear model (HLM) was used. The significance of the relationship between change in electrode depth and change in RF location (i.e., slope) was tested individually for each condition (i.e., whether slope of HLM was horizontal). Changes in the relationship between electrode depth and change in RF location were then compared across treatments via the interaction term for each axis of visual space to determine the effects of early retinal wave blockade on fine-scale retinotopy.

ACKNOWLEDGMENTS. We thank W. M. Usrey, M. E. Burns, M. D. Wilson, and M. B. Feller for feedback on the manuscript, M. D. Wilson for help with statistical analyses, and D. J. Sperka for technical support for visual electrophysiology experiments. Research was supported by US National Eye Institute Grants EY011369, EY015387, and EY03991 and US National Center for Advancing Translational Sciences Grant TR000002. This article is dedicated in remembrance of Dr. Barbara Chapman.

1. Huberman AD, Feller MB, Chapman B (2008) Mechanisms underlying development of visual maps and receptive fields. *Annu Rev Neurosci* 31:479–509.
2. Cang J, Feldheim DA (2013) Developmental mechanisms of topographic map formation and alignment. *Annu Rev Neurosci* 36:51–77.
3. Pfeiffenberger C, et al. (2005) Ephrin-As and neural activity are required for eye-specific patterning during retinogeniculate mapping. *Nat Neurosci* 8(8):1022–1027.
4. Huberman AD, Murray KD, Warland DK, Feldheim DA, Chapman B (2005) Ephrin-As mediate targeting of eye-specific projections to the lateral geniculate nucleus. *Nat Neurosci* 8(8):1013–1021.
5. Leamey CA, et al. (2007) Ten_m3 regulates eye-specific patterning in the mammalian visual pathway and is required for binocular vision. *PLoS Biol* 5(9):e241.
6. Cang J, et al. (2008) Selective disruption of one Cartesian axis of cortical maps and receptive fields by deficiency in ephrin-As and structured activity. *Neuron* 57(4): 511–523.
7. Guillery R, LaMantia A, Robson J, Huang K (1985) The influence of retinal afferents upon the development of layers in the dorsal lateral geniculate nucleus of mustelids. *J Neurosci* 5(5):1370–1379.
8. Penn AA, Riquelme PA, Feller MB, Shatz CJ (1998) Competition in retinogeniculate patterning driven by spontaneous activity. *Science* 279(5359):2108–2112.
9. Morgan J, Thompson ID (1993) The segregation of ON- and OFF-center responses in the lateral geniculate nucleus of normal and monocularly enucleated ferrets. *Vis Neurosci* 10(2):303–311.
10. Thompson ID, Morgan JE, Henderson Z (1993) The effects of monocular enucleation on ganglion cell number and terminal distribution in the ferret's retinal pathway. *Eur J Neurosci* 5(4):357–367.
11. Dhande OS, et al. (2011) Development of single retinofugal axon arbors in normal and β2 knock-out mice. *J Neurosci* 31(9):3384–3399.
12. Xu HP, et al. (2011) An instructive role for patterned spontaneous retinal activity in mouse visual map development. *Neuron* 70(6):1115–1127.
13. Ackman JB, Burbridge TJ, Crair MC (2012) Retinal waves coordinate patterned activity throughout the developing visual system. *Nature* 490(7419):219–225.
14. Zhang J, Ackman JB, Xu HP, Crair MC (2012) Visual map development depends on the temporal pattern of binocular activity in mice. *Nat Neurosci* 15(2):298–307.
15. Kirkby LA, Sack GS, Firl A, Feller MB (2013) A role for correlated spontaneous activity in the assembly of neural circuits. *Neuron* 80(5):1129–1144.
16. Wong RO, Meister M, Shatz CJ (1993) Transient period of correlated bursting activity during development of the mammalian retina. *Neuron* 11(5):923–938.
17. Feller MB, Wellis DP, Stellwagen D, Werblin FS, Shatz CJ (1996) Requirement for cholinergic synaptic transmission in the propagation of spontaneous retinal waves. *Science* 272(5265):1182–1187.
18. Sun C, Speer CM, Wang GY, Chapman B, Chalupa LM (2008) Epibatidine application in vitro blocks retinal waves without silencing all retinal ganglion cell action potentials in developing retina of the mouse and ferret. *J Neurophysiol* 100(6):3253–3263.
19. Hebb DO (1949) *The Organization of Behavior: A Neuropsychological Theory* (Wiley, New York).
20. Butts DA, Kanold PO, Shatz CJ (2007) A burst-based "Hebbian" learning rule at retinogeniculate synapses links retinal waves to activity-dependent refinement. *PLoS Biol* 5(3):e61.
21. Stellwagen D, Shatz CJ (2002) An instructive role for retinal waves in the development of retinogeniculate connectivity. *Neuron* 33(3):357–367.
22. Grubb MS, Rossi FM, Changeux JP, Thompson ID (2003) Abnormal functional organization in the dorsal lateral geniculate nucleus of mice lacking the beta 2 subunit of the nicotinic acetylcholine receptor. *Neuron* 40(6):1161–1172.
23. Linden DC, Guillery RW, Cucchiaro J (1981) The dorsal lateral geniculate nucleus of the normal ferret and its postnatal development. *J Comp Neurol* 203(2):189–211.
24. Hutchins JB, Casagrande VA (1990) Development of the lateral geniculate nucleus: Interactions between retinal afferent, cytoarchitectonic, and glial cell process lamination in ferrets and tree shrews. *J Comp Neurol* 298(1):113–128.
25. Speer CM, Mikula S, Huberman AD, Chapman B (2010) The developmental remodeling of eye-specific afferents in the ferret dorsal lateral geniculate nucleus. *Anat Rec (Hoboken)* 293(1):1–24.
26. Huberman AD, Stellwagen D, Chapman B (2002) Decoupling eye-specific segregation from lamination in the lateral geniculate nucleus. *J Neurosci* 22(21):9419–9429.

27. Muir-Robinson G, Hwang BJ, Feller MB (2002) Retinogeniculate axons undergo eye-specific segregation in the absence of eye-specific layers. *J Neurosci* 22(13):5259–5264.
28. Ruthazer ES, Cline HT (2004) Insights into activity-dependent map formation from the retinotectal system: A middle-of-the-brain perspective. *J Neurobiol* 59(1):134–146.
29. Gaze RM, Sharma (1970) Axial differences in the reinnervation of the goldfish optic tectum by regenerating optic nerve fibres. *Exp Brain Res* 10(2):171–181.
30. Yoon M (1971) Reorganization of retinotectal projection following surgical operations on the optic tectum in goldfish. *Exp Neurol* 33(2):395–411.
31. Schimidt JT, Cicerone CM, Easter SS (1978) Expansion of the half retinal projection to the tectum in goldfish: An electrophysiological and anatomical study. *J Comp Neurol* 177(2):257–277.
32. Udin SB, Gaze RM (1983) Expansion and retinotopic order in the goldfish retinotectal map after large retinal lesions. *Exp Brain Res* 50(2-3):347–352.
33. Speer CM, et al. (2014) Eye-specific retinogeniculate segregation proceeds normally following disruption of patterned spontaneous retinal activity. *Neural Dev* 9(1):25.
34. Mullen RJ, Buck CR, Smith AM (1992) NeuN, a neuronal specific nuclear protein in vertebrates. *Development* 116(1):201–211.
35. Henderson Z, Finlay B, Wikler K (1988) Development of ganglion cell topography in ferret retina. *J Neurosci* 8(4):1194–1205.
36. Reid RC, Victor JD, Shapley RM (1997) The use of m-sequences in the analysis of visual neurons: Linear receptive field properties. *Vis Neurosci* 14(6):1015–1027.
37. Tavazoie SF, Reid RC (2000) Diverse receptive fields in the lateral geniculate nucleus during thalamocortical development. *Nat Neurosci* 3(6):608–616.
38. Speer CM, Sun C, Chapman B (2011) Activity-dependent disruption of intersublaminar spaces and ABAKAN expression does not impact functional on and off organization in the ferret retinogeniculate system. *Neural Dev* 6(1):7.
39. Chandrasekaran AR, Plas DT, Gonzalez E, Crair MC (2005) Evidence for an instructive role of retinal activity in retinotopic map refinement in the superior colliculus of the mouse. *J Neurosci* 25(29):6929–6938.
40. Zahs KR, Stryker MP (1985) The projection of the visual field onto the lateral geniculate nucleus of the ferret. *J Comp Neurol* 241(2):210–224.
41. Lee H, et al. (2014) Synapse elimination and learning rules co-regulated by MHC class I H2-D. *Nature* 509(7499):195–200.
42. Sretavan DW, Shatz CJ (1986) Prenatal development of cat retinogeniculate axon arbors in the absence of binocular interactions. *J Neurosci* 6(4):990–1003.
43. Wefers CJ, Dehay C, Berland M, Kennedy H, Chalupa LM (2000) Binocular competition does not regulate retinogeniculate arbor size in fetal monkey. *J Comp Neurol* 427(3): 362–369.
44. Garraghty PE, Shatz CJ, Sretavan DW, Sur M (1988) Axon arbors of X and Y retinal ganglion cells are differentially affected by prenatal disruption of binocular inputs. *Proc Natl Acad Sci USA* 85(19):7361–7365.
45. Vitek DJ, Schall JD, Leventhal AG (1985) Morphology, central projections, and dendritic field orientation of retinal ganglion cells in the ferret. *J Comp Neurol* 241(1): 1–11.
46. Torborg CL, Hansen KA, Feller MB (2005) High frequency, synchronized bursting drives eye-specific segregation of retinogeniculate projections. *Nat Neurosci* 8(1): 72–78.
47. Demas J, et al. (2006) Failure to maintain eye-specific segregation in nob, a mutant with abnormally patterned retinal activity. *Neuron* 50(2):247–259.
48. Koch SM, et al. (2011) Pathway-specific genetic attenuation of glutamate release alters select features of competition-based visual circuit refinement. *Neuron* 71(2): 235–242.
49. Nicol X, et al. (2007) cAMP oscillations and retinal activity are permissive for ephrin signaling during the establishment of the retinotopic map. *Nat Neurosci* 10(3): 340–347.
50. Dunn TA, et al. (2006) Imaging of cAMP levels and protein kinase A activity reveals that retinal waves drive oscillations in second-messenger cascades. *J Neurosci* 26(49): 12807–12815.
51. Benjumeda I, et al. (2013) Uncoupling of EphA/ephrinA signaling and spontaneous activity in neural circuit wiring. *J Neurosci* 33(46):18208–18218.
52. Chapman B (2000) Necessity for afferent activity to maintain eye-specific segregation in ferret lateral geniculate nucleus. *Science* 287(5462):2479–2482.
53. Grubb MS, Thompson ID (2004) Visual response properties in the dorsal lateral geniculate nucleus of mice lacking the beta2 subunit of the nicotinic acetylcholine receptor. *J Neurosci* 24(39):8459–8469.
54. Kawasaki H, Crowley JC, Livesey FJ, Katz LC (2004) Molecular organization of the ferret visual thalamus. *J Neurosci* 24(44):9962–9970.
55. Robson JA, Geisert EE, Jr (1994) Expression of a keratin sulfate proteoglycan during development of the dorsal lateral geniculate nucleus in the ferret. *J Comp Neurol* 340(3):349–360.
56. Wang L, et al. (2009) Direction-specific disruption of subcortical visual behavior and receptive fields in mice lacking the beta2 subunit of nicotinic acetylcholine receptor. *J Neurosci* 29(41):12909–12918.
57. Cai D, Cohen KB, Luo T, Lichtman JW, Sanes JR (2013) Improved tools for the Brainbow toolbox. *Nat Methods* 10(6):540–547.
58. Chalupa LM (2009) Retinal waves are unlikely to instruct the formation of eye-specific retinogeniculate projections. *Neural Dev* 4:25.
59. Feller MB (2009) Retinal waves are likely to instruct the formation of eye-specific retinogeniculate projections. *Neural Dev* 4:24.
60. Huberman AD, Speer CM, Chapman B (2006) Spontaneous retinal activity mediates development of ocular dominance columns and binocular receptive fields in v1. *Neuron* 52(2):247–254.
61. Schindelin J, et al. (2012) Fiji: An open-source platform for biological-image analysis. *Nat Methods* 9(7):676–682.